Proceedings of the 26th International Conference on
Port and Ocean Engineering under Arctic Conditions
June 14-18, 2021, Moscow, Russia

Investigation of Thermal Ice Pressure Loads by Laboratory Measurements

Patrik Buil[1], Christian Schröder[2], Nils Reimer[3]

[1] HSVA & University of Duisburg-Essen, Hamburg, Germany

[2] HSVA, Hamburg, Germany

[3] HSVA, Hamburg, Germany

ABSTRACT

In areas where naval structures possibly restrict the deformation of ice covers thermal ice loads are one of the major design-loads. Structures that are most likely concerned are dams, bridges, port walls, offshore structures, watertanks on-board of ships and non-moving ship-hulls under arctic conditions. Based on full scale measurements, regulations for the design of dams and bridges suggest considering a relative wide range of loads ranging between 50-750 kN/m depending on the source. Since the event of deformation of ice is a complex process depending on various key parameters, this paper discusses investigations done under laboratory conditions to gain a better understanding of the influence of each parameter. A test set up was built and equipped with sensors to measure the local pressure distribution and the global forces on the ice confined set up. Compared to full-scale measurements, the controlled environment enables a better insight on the influence of particular key parameters. The paper as well discusses the influence from the water salinity on the resulting force levels. Furthermore, a new experimental investigation was made to take into account for the elasticity of the ice confined body. The aim of this paper is to better understand the reported full-scale measurements by tests under a controlled environment.

Thermal; Ice; Pressure; Experimental; Laboratory

INTRODUCTION

The existence of thermal ice pressure is known for a long time, yet not all mechanisms behind this phenomenon are well understood. Regulations for the design of structures in arctic environment consider thermal ice pressure as part of static ice loads, but because of many different key parameters that influence such events, there is no golden rule to predict thermal ice loads accurately. This leads to a relative wide range of loads ranging between 50-750 kN/m depending on the source (Alexy, 1998). As a consequence, some structures may be oversized, which leads to higher investment costs, and some structures may be undersized, which can lead to damages and failure of the structure. Various field measurements have been carried out and analyzed by (Comfort et al., 2003), (Fransson, 1988), (Cox, 1984), (Watts et al., 1976), and (Bergdahl and Wernersson, 1978), but since the maximum thermal ice loads only occur only under very rare weather conditions, the measurement duration must be very long to increase the odds to capture valuable data. Laboratory conditions allow to shorten the measurement duration by replicating the same extreme conditions in a controlled environment. Compared to field measurement methods, another advantage of the controlled environment is the deletion of non-thermal influences on the measurement, such as tidal hub or drift forces. This enables a better insight on the influence of particular key parameters in the process of thermal ice pressure. This paper presents new experimental investigations that have been carried under laboratory conditions during the German research Project "Megayachtschaum". The experiment has been executed in the Arctic Environmental Test Basin (AETB) at the Hamburg Ship Model Basin. In the test facility housing a basin of 30m*6m*1,5m (L*B*H), the air temperature can be regulated between -15°C to + 15°C and ice growth rates up to ~2 mm/h are possible. For this experiment, a customized test set up was created and installed on the basin wall. With this set-up, a small and a big plate are used as test specimen on which the global and local forces are measured. The steel plates are coated with a special foam developed during the research project. One target of the test campaign is to see if this material is suitable for arctic conditions and strong enough to withstand the thermal ice pressure. Sensors capture the temperature profile of the air, ice and water at three different locations. The tests were performed with freshwater (FW) and saltwater (SW). In this paper both results will be presented, but since previous works state that the largest pressure magnitudes can be expected in freshwater (Marchenko, 2018), the main focus will be kept on the results of the FW test. A further test was performed in order to quantify the effects on the results of the overall stiffness of the used test set-up itself. Therefore, the part of the set-up with the small test specimen was taken to measure the deformation while forces were applied with similar magnitude as the measured forces in the thermal ice pressure tests. The aim of this paper is to introduce a new experimental investigation under laboratory conditions and to show the influence of particular key parameters on thermal ice pressure.

Experimental Set-Up

Ошибка! Источник ссылки не найден. shows a 3-D image of the test set-up and its

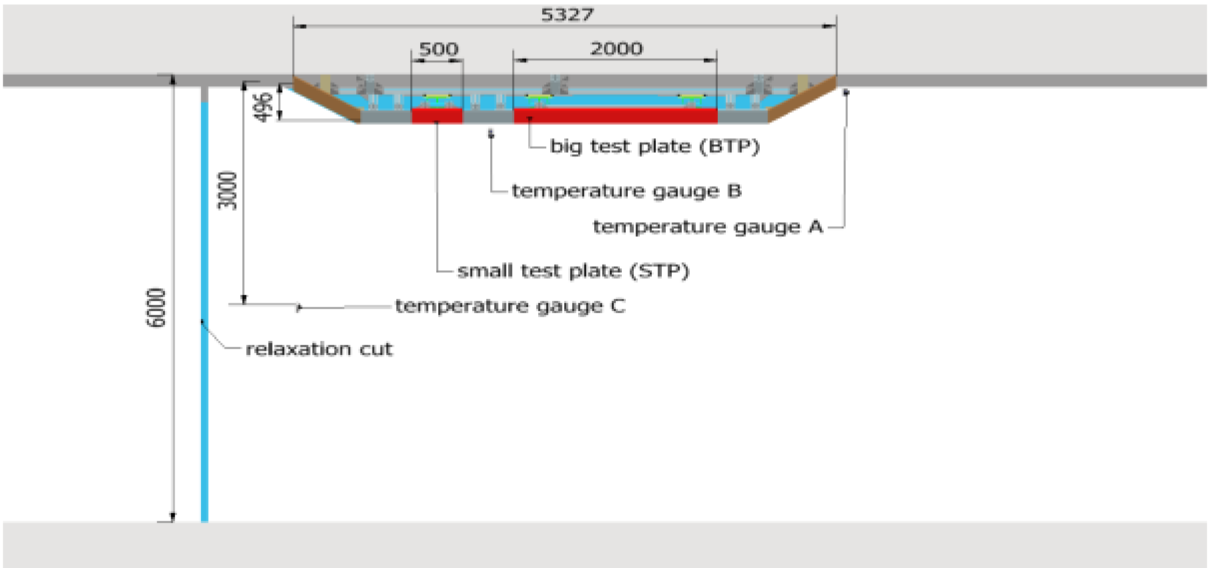

Fig. 1: 3-D Image of the experimental set-up

dimensions in mm. The 500 mm high and 20 mm thick test plates are indicated in red. Due to their different width of 500 mm and 2000 mm, the left and right plate are referred as the small test plate (STP) and the big test plate (BTP), respectively. One load cell is attached to the STP and two load cells are attached parallel to the BTP in order to measure the global forces on both plates. Three temperature gauges were used at the positions A, B and C (see **Ошибка! Источник ссылки не найден.**). Each temperature gauge is equipped with eight sensors in certain distances. To capture the local pressure distribution, three sensor mats were used, one on each specimen and one on the basin wall, as shown in **Ошибка! Источник ссылки не найден.**.

Fig. 2: Experimental set-up

Experimental Procedure

An overview of the experimental procedure and its duration is given in **Ошибка! Источник ссылки не найден.**.

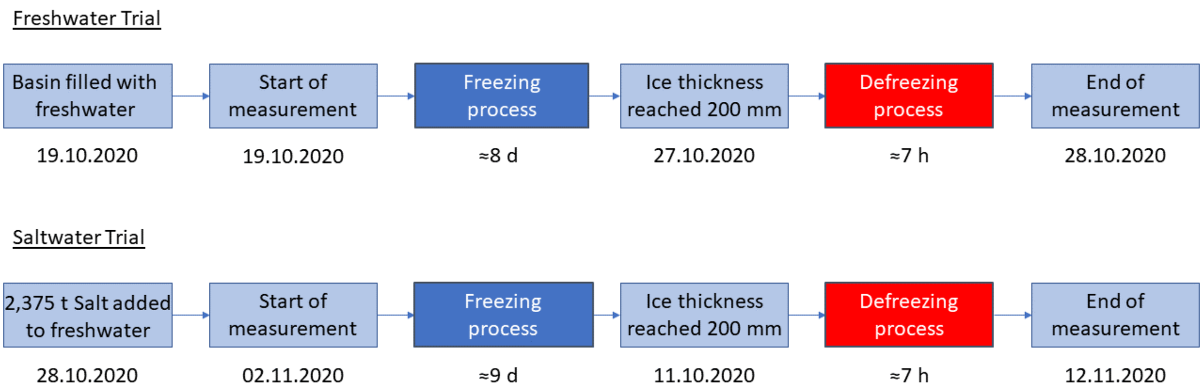

Fig. 3: Overview of the experimental procedure

The two main steps, the freezing and the de-freezing process, are indicated in blue and red, respectively. In the first test, the basin was filled with freshwater. The temperature gauges were placed at the water surface, so that once a test ice thickness of 200 mm is reached, two of the eight sensors will be on top of the ice layer, two will be in the ice layer and four of them in the water. Temperature gauge A was placed right in front of the basin wall, temperature gauge B right in front of the set-up between the two specimen and temperature gauge A was placed in the middle of the basin (see **Ошибка! Источник ссылки не найден.**). The measurement starts with the freezing process. Therefore, the air temperature in the facility was cooled down to ≈-15°C. During the freezing process, the ice thickness was measured in regular intervals and the area behind the set-up was kept ice free, so that deformations in direction of the basin wall are not restricted. Once the test ice thickness was reached, a cut in the ice was made to relief the strain and at the same time the de-freezing process was initiated. Therefore, the cooling devices are turned off and a sudden temperature rise is achieved by circulating warm air from the outside through the facility. The measurements were stopped after seven hours of de-freezing. After the freshwater test, the experiment was repeated in the same manner with saltwater with a salinity of 10.8‰, which is a typical value surface salinity of brackish water in Northern-European seas (Madsen and Højerslev, 2009).

Boundary Conditions

Like any solid body, the heating of ice leads to its expansion. This is what makes the de-freezing process of main interest since the restriction of the expansion causes thermal ice pressure. This section shows the boundary conditions that were achieved at the moment, the de-freezing process was initiated.

Table 1: Boundary conditions

		FW	SW
Ice Thickness	[mm]	200	200
Ice Temperature at the surface/Air Temperature	[°C]	-15.045	-13.774
Ice Temperature at 55 mm depth	[°C]	-4.943	-5.725
Ice Temperature at 105 mm depth	[°C]	-3.604	-4.331
Water Temperature	[°C]	-0.3290	-0.6360
FDH	[°C]	2995	3005
Salinity	[‰]	0	10.8

Table 1 sums up the boundary conditions for the FW and SW tests. In both tests the de-freezing process was initiated when the ice reached a thickness of 200 mm. The temperature differences of the air and the ice between both tests were less than 2°C. The freezing process is consolidated as freezing degree hours (FDH), which is the accumulation of the hourly mean temperature $\bar{T}_i$ until the target ice thickness of 200 mm is reached. With Δt =1 h, FDH can be written as the following:

$$FDH = -\sum \bar{T}_i \cdot \Delta t \tag{1}$$

Compared to freshwater, saltwater has a lower freezing point and a lower thermal conductivity due to disorder in the crystalline structure of the ice. The reduction of thermal conductivity is nearly a factor of two near the top surface of the ice. Deeper in the ice, in contrast, heat flow is enhanced by a contribution from brine convection (Trodahl et al., 2001). These saltwater characteristics lead to a slightly higher FDH value for the saltwater freezing process. According to (B. Lishman and A. Marchenko, 2014), the coefficient of thermal expansion is around $\alpha_t = 50 \cdot 10^{-6}\ [°C^{-1}]$ for fresh- and saltwater. Ice naturally exists at a temperature that is very close to its melting point. Therefore, the 2019 edition of ISO 19906 recommends the usage of an 'effective' modulus. It implies that the deformation is not only elastic, but also comprises timedependent recoverable strain, and non-elastic non-recoverable deformation. According to the International Organization for Standardization (ISO/FDIS 19906), the effective Young's modulus of ice can be written as:

$$E_f = 5.31 - 0.436 v_b^{0.5} \tag{2}$$

, with the liquid brine content v_b in ppt.
Determined by Eq. (2), the effective Young's modulus was $E_{f\,FW} = 5.31$ [GPa] for the ice in the FW test and $E_{f\,SW} = 3.93$ [GPa] in the SW test.

RESULTS

Comparing the recorded air temperature profile during the FW and SW tests, one can see that laboratory conditions enable a good repeatability of temperature events. Similar initial conditions were achieved at the beginning of the de-freezing process and also the temperature gradient and the total temperature difference during the de-freezing process match well in both tests, as shown in **Ошибка! Источник ссылки не найден.**.

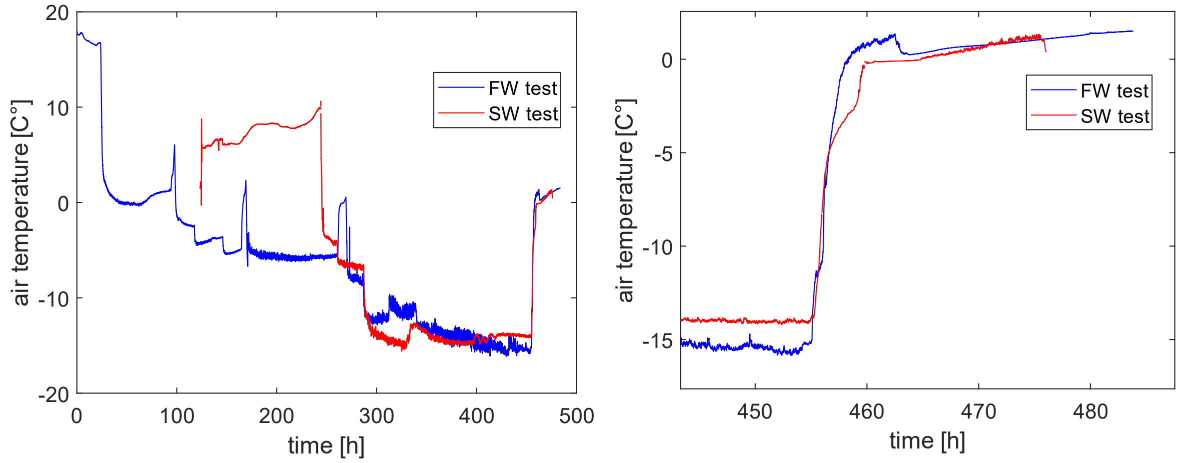

a) b)

Fig. 4: Air Temperature Profile during FW Test

In Fig. *4* a), the air temperature during the whole experiment is shown, while Fig. *4* b) gives a closer look on the temperature profile during the de-freezing process. In the first few hours after initiating the de-freezing process, the air temperature gradients approach almost constant values of $\dot{T}_{FW} = 5.86\,{}^{K}/_{h}$ and $\dot{T}_{SW} = 5.30\,{}^{K}/_{h}$ before they decrease. The time to reach the melting point air temperature (≈0°C for FW and ≈-6°C for SW with a salinity of 10.8 ‰) is 3.17 h and 1.05 h for FW and SW, respectively. Fig. 5 shows the temperature over the ice thickness after certain hours after the beginning of the de-freezing process in the FW test. The original data shows the temperature at four discrete points, at the ice surface, 55 mm and 105 mm below the surface and at the ice bottom, whereby the boundary conditions were assumed, that the ice surface temperature equals the air temperature and that the ice bottom temperature

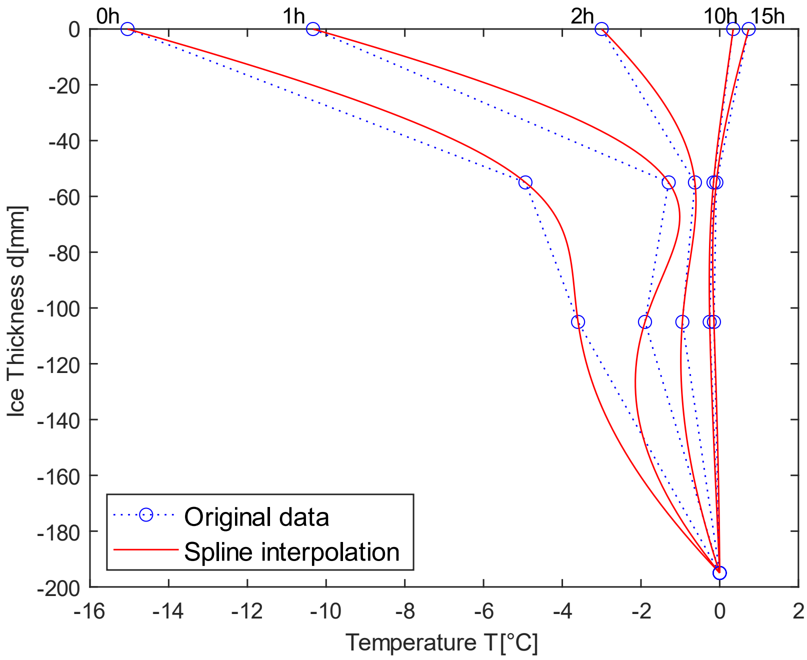

Fig. 5: Temperature over ice thickness after the beginning of de-freezing

equals the melting point temperature. The temperature between two data points was calculated with a spline interpolation. Fig. 6 shows the air temperature profile and the forces on the STP and BTP during the freshwater test two hours before and 15 hours after the beginning of the de-freezing process. Distorted measurements caused by temporary working missions are indicated as disturbed data in black. The working missions included the removal of ice behind the specimen, as well as a relaxation cut in the ice sheet a few meters aside the test set-up (see

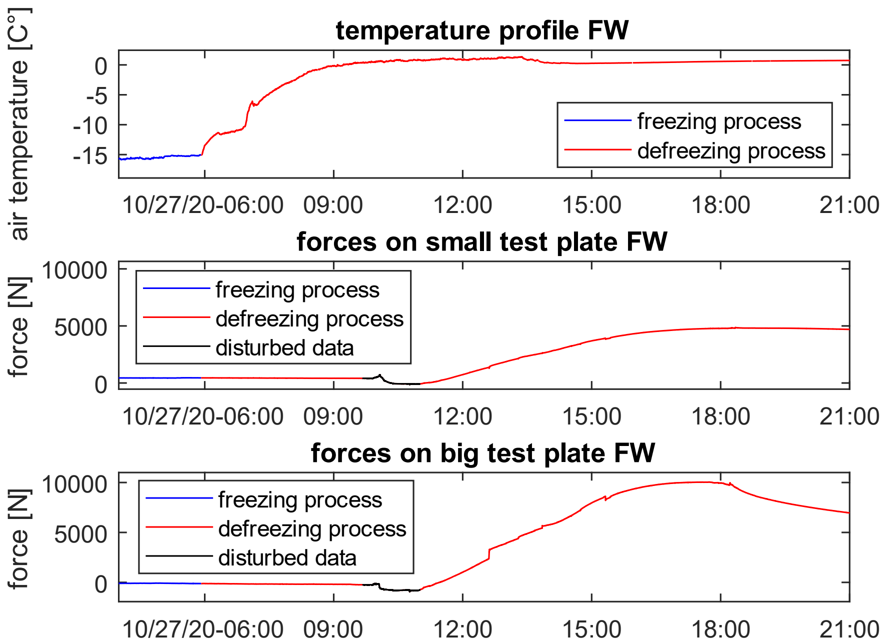

Fig. 6: Temperature and force profiles during the FW test

Fig. 1). It can also be seen in a drop of forces on the test plates at around 10.30 AM. A time dilatation of approximately five hours can be seen between the start of de-freezing and the increase of force, which can be related to the thermal conductivity of the ice. The measured maximum forces occurred after 12.42 h on the STP and after 11.72 h on the BTP in the FW test. In the SW test the maximum forces were reached after 4.82 h and 6.47 h, respectively and the magnitude appeared roughly ten times lower than in the FW test. Comparing the measured forces on the STP and the BTP in the FW test, it can be seen that maximum forces on the BTP are roughly twice the magnitude of the ones on the STP (see Fig. 6), which could also be observed in SW test. Reason for this might be the (unknown) horizontal distribution of the thermal ice pressure. There are two main factors that contribute to the horizontal pressure distribution. On the one hand, the pressure distribution is affected by the basin walls', wooden frames' and test plates' different stiffness. Areas with higher stiffness lead to local pressure peaks, while areas with a lower stiffness cause pressure relaxation. As a result, high pressure gradients are expected at the transitions between the basin wall and the wooden frames and at the transition between the wooden frames and the test plates. The latter transition might have the strongest effect on the results, since the wooden frames are much stiffer than the test plates and therefore, we assume that a reasonable amount of force could not be measured because it was absorbed by the surrounding wooden frames. Even though the BTPs' stiffness was increased with a longitudinal frame on the backside of the plate between the two load cells, we can only hypothesize how much pressure relaxation due to bending and displacement took place and how the pressure accordingly distributed on the test plates. Therefore, Fig. *7* shows two schematic drawings, a) and b), of hypothetical pressure distributions, but the truth might lie somewhere in between.

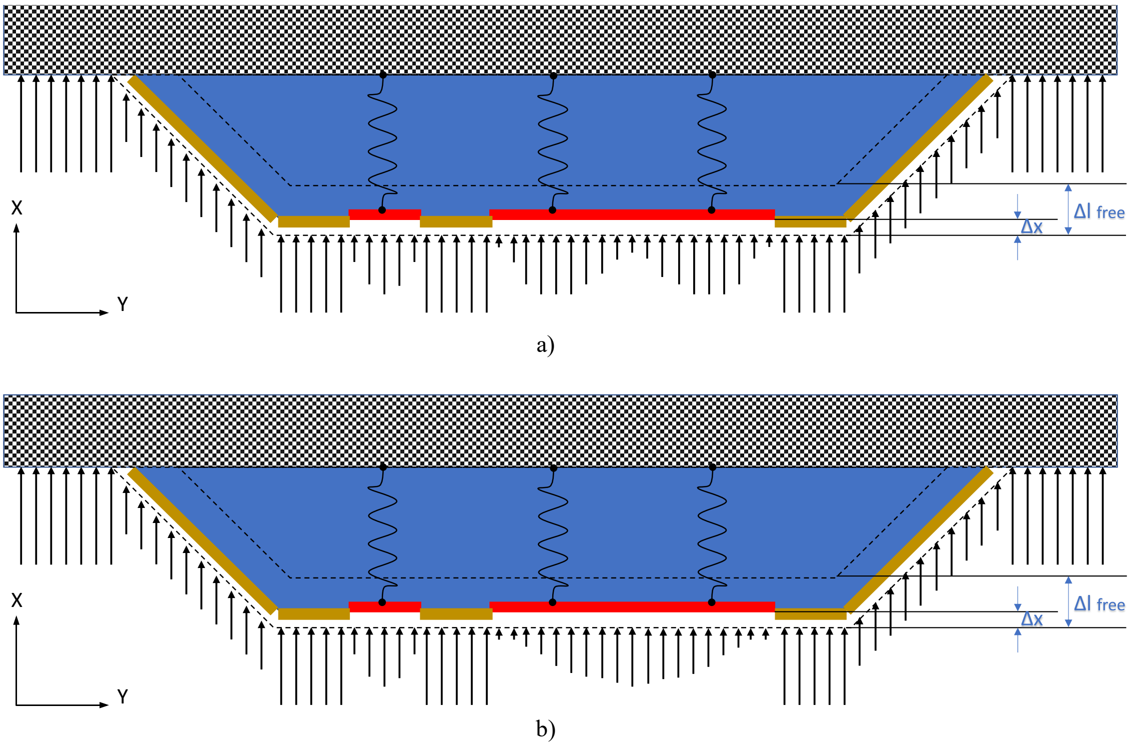

Fig. 7: Schematic pressure distribution

On the other hand, the pressure distribution is affected by the contact area. Pressure-area curves as revised by (Masterson et al., 2007), show a pressure decrease with growing contact area. With a pressure-area curve according to the ISO 19906 (ISO/FDIS 19906), the relation between the design pressure P and the contact area A is given as following:

$$P(A) = 7.4 \cdot A^{-0.7} \quad (3)$$

With the assumption of a full contact area ($A_{STP} = 0.1\, m^2$; $A_{BTP} = 0.4\, m^2$), the measured forces lead to global pressures of 43.63 kPa on the STP and 25.11 kPa on the BTP, which indicates a pressure reduction of 42.45 % on the BTP. The same assumption for the area in Eq. (3) leads to a pressure reduction of 62.1% on the BTP with respect to the STP. However, based on this pressure-area curve we can only state the reduction of the pressure on the BTP compared to the STP, but the actual effective pressure is not known. Recommendations for assessing thermal ice action effects are covered in the ISO 19906 based on Franssons (1988) rheologic prediction model. Further theories to predict thermal ice loads have been proposed by the Russian SN-76-66 code (Belkov, 1973), Rose (1947), Xu Bomeng (1981, 1986) and M. Drouin and B. Michel (1974). The latter two models are limited for ice thicknesses of 0.4 m or larger. For smaller ice thickness the maximum pressures can be obtained from extending the derived pressure-ice thickness curves. The calculated thermal loads for the boundary conditions of the FW test and the measured loads are given in Table 2.

Table 2: Calculated and. measured thermal ice loads

	ISO 19906	SN 76-66	Rose	Xu Bomeng	Drouin and Michel	Test Results STP	Test Results BTP
Thermal Ice Load [kN/m]	83.41	83.52	36.49	24.53	73.58	9.73	5.02

It can be seen, that all models overpredict the measured loads, which seems reasonable when predicting design loads for structures. Nevertheless, the loads according to the ISO 19906 and the SN 76-66 extremely overpredict this load case, but they are in very good agreement with each other. Xu Bomengs and Roses models seem to fit the measured data best, but the accuracy is still far from good. One reason why the measured loads are significantly smaller than predicted loads might be the pressure absorption of the set-up. As mentioned earlier the stiffness of the wooden frames is higher than the stiffness of the test plates that are attached to load cells. Therefore, the wooden frames might restrict a significant amount of the thermal ice expansion, which is then not measured with the load cell. Further analysis of the pressure mat sensors is planned to get a better understanding of the pressure distribution during this experiment. Moreover, the influence of the set-ups stiffness needs to be taken into account. Therefore, another experiment was executed in which the displacement of the part of the set up with the STP was measured depending on the applied force in order to determine the stiffness k of the used test set-up, as shown in Fig. 8. Figure Fig. 8 a) shows a picture of the experimental set-up while Figure Fig. 8 b) shows the measured data. The displacement caused by the measured forces in both test trails are given in Table 3.

b)

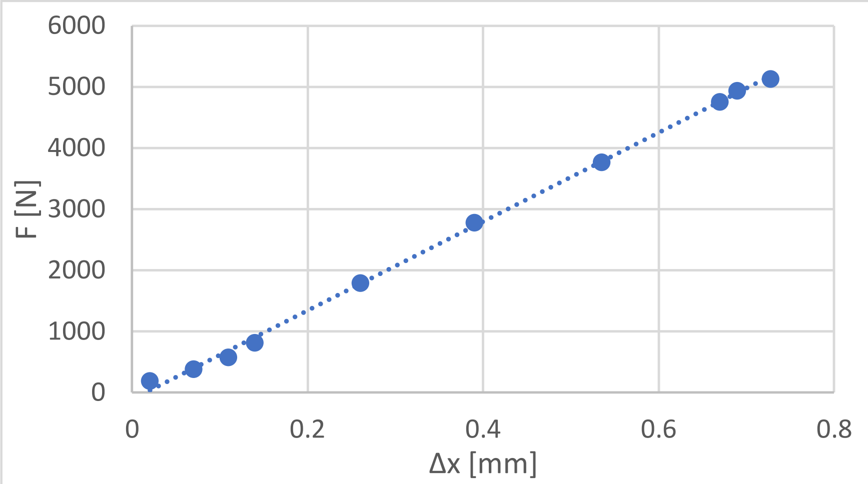

b)

Fig. 8: Experiment to determine the stiffness of the set-up

Table 3: Measured and calculated forces

	specimen	$F_{measured}$ $[kN]$	Δx $[mm]$
FW	STP	4.8629	0.670
	BTP	10.0413	0.691
SW	STP	0.4109	0.057
	BTP	0.7461	0.051

CONCLUSIONS

In this paper a new experimental investigation on thermal ice pressure under laboratory conditions was presented. A test set-up was built, similar to the set-up that was used in field measurements by (Malm et al., 2017). An ice sheet with a thickness of 200 mm was frozen and de-frozen in fresh- and saltwater the thereby measured forces and temperatures were presented. Our measurements confirmed that thermal loads decrease significantly with salinity. We also found that the measured forces appear very small compared to theoretical calculated values. As reason for this, we discussed the pressure distribution which is highly effected by the presence of the surrounding structure and its' varying stiffness. These founding's transferred to offshore structures or ships could assist to adapt the design loads for stiffer and less stiff areas.

As a next step we plan to evaluate the results from the pressure mat sensors that were used during both tests to get a clearer view on the pressure distribution and therefore a better understanding of the resulting forces.

ACKNOWLEDGEMENT

The author is grateful for the funding of the tests and evaluations by the German Federal Ministry for Economic Affairs and Energy (BMWi) through the project MegaYachtSchaum (03SX440B).

References

Alexy, M. (1998) *Eisdruck auf Kanalbrücken: Ice Pressure on Canal Bridges* 79.

B. Lishman and A. Marchenko (2014) 'An investigation of relative thermal expansion and contraction of ice and steel'.

Belkov, G. (1973) 'Instructions for Determining Ice Loads on River Structures (SN 76-66): Technical Translation 1663', *National Research Counsil of Canada*.

Bergdahl, L. and Wernersson, L. (1978) 'Calculated and Expected Thermal Ice Pressures in Five Swedish Lakes'.

Comfort, G., Gong, Y., Singh, S. and Abdelnour, R. (2003) 'Static ice loads on dams', *Canadian Journal of Civil Engineering*, vol. 30, no. 1, pp. 42–68.

Cox, G. (1984) 'A preliminary investigation of thermal ice pressures', *Cold Regions Science and Technology*, vol. 9, pp. 221–229.

Fransson, L. (1988) 'Thermal Ice Pressure on Structures in Ice Covers' [Online]. Available at https://books.google.de/books?id=-tCgHAAACAAJ.

ISO/FDIS 19906: *Petroleum and natural gas industries - Arctic offshore structures.*

M. Drouin and B. Michel (1974) 'Pressures of Thermal Origin Exerted by Ice Sheets upon Hydraulic Structures (Les Poussees d'Origine Thermique Exercees par les Couverts de Glace sur les Structures Hydrauliques)'.

Madsen, K. and Højerslev, N. (2009) 'Long-term temperature and salinity records from the Baltic Sea transition zone', *Boreal Environment Research*, vol. 14, pp. 125–131.

Malm, R., Fransson, L., Nordström, E., Westberg Wilde, M., Johansson, F. and Hellgren, R. (2017) *Load conditions for Ice Loads*.

Marchenko, A. (2018) 'Thermo-mechanical loads of confined sea ice on structures | Philosophical Transactions of the Royal Society A: Mathematical, Physical and Engineering Sciences' [Online]. Available at https://royalsocietypublishing.org/doi/10.1098/rsta.2017.0341 (Accessed 23 March 2021).

Masterson, D. M., Frederking, R., Wright, B., Karna, T. and Maddock, W. P. (2007) 'A revised ice pressure-area curve', *Proceedings of the International Conference on Port and Ocean Engineering under Arctic Conditions, POAC*, pp. 305–314.

Rose, E. (1947) 'Thrust Exerted by Expanding Ice Sheet', *Transactions of the American Society of Civil Engineers*, vol. 112, no. 1, pp. 871–885.

Trodahl, H. J., Wilkinson, S. O. F., McGuinness, M. J. and Haskell, T. G. (2001) 'Thermal conductivity of sea ice; dependence on temperature and depth', *Geophysical Research Letters*, vol. 28, no. 7, pp. 1279–1282.

Watts, F. J., Podolny, W. and United States. Federal Highway Administration. Bridge Division (1976) *Ice Loads on Bridge Piers* [Online], Federal Highway Administration. Available at https://books.google.de/books?id=bZTbeDMkzecC.

Xu Bomeng (1981) 'Pressure Due to Expansion of Ice Sheet in Reservoirs', *IAHR Symposium on Ice*, pp. 540–550.

Xu Bomeng (1986) 'Design Value of Pressure Due to Expansion of Ice Sheet in Reservoir', *IAHR Symposium on Ice*, pp. 231–238.